Pergamon

Acta mater. Vol. 46, No. 13, pp. 4519–4525, 1998

Printed in Great Britain

PII: S1359-6454(98)00156-6

1359-6454/98 $19.00 + .00

STRUCTURAL AND HYDRIDING PROPERTIES OF $(Mg_{1-x}Al_x)Ni$–H(D) WITH AMORPHOUS OR CsCl-TYPE CUBIC STRUCTURE (x = 0–0.5)

S. ORIMO[1]†‡, K. IKEDA[1]§, H. FUJII[1], S. SARUKI[2], T. FUKUNAGA[2]¶, A. ZÜTTEL[3] and L. SCHLAPBACH[3]

[1]Faculty of Integrated Arts and Sciences, Hiroshima University, Higashi-Hiroshima 739, Japan, [2]Faculty of Engineering, Nagoya University, Nagoya 464-01, Japan and [3]University of Fribourg, Physics Institute, Perolles CH-1700, Switzerland

(Received 25 February 1998; accepted 14 April 1998)

Abstract—The amorphous phase is formed in $(Mg_{1-x}Al_x)Ni$ with x = 0–0.2, while the crystalline phase of a CsCl-type cubic structure is formed with x = 0.3–0.5 even in the as-mechanically-alloyed states. The total radial distribution functions for X-ray and neutron diffractions show that deuterium in MgNi, that is, x = 0, occupies the interstitial tetrahedral site composed of nearly 2Mg2Ni. Electrochemical *P–C* (hydrogen pressure–composition) isotherm measurements revealed that there is an obvious miscibility-gap pressure higher than 10^{-4} MPa at room temperature even in MgNi, and that the pressure increases by the Al substitution. © *1998 Acta Metallurgica Inc. Published by Elsevier Science Ltd. All rights reserved.*

1. INTRODUCTION

There are two intermetallic compounds in the Mg–Ni binary system, that is, Mg_2Ni and $MgNi_2$ [1]. Upon hydrogenation, the former Mg_2Ni transforms into the hydride phase Mg_2NiH_4, so as to form a stable covalent-type bonding composed of Mg^{2+} and $[NiH_4]^{4-}$ complex [2–5]. On the other hand, the latter $MgNi_2$ does not react with hydrogen at least in the crystalline phase [6].

In the equiatomic composition between the two compounds mentioned above, the amorphous MgNi phase is formed by mechanical alloying [7–13]. The maximum hydrogen content in MgNi corresponds to a composition of $MgNiH_{1.9}$; the pressure dependence of the hydrogen content is small compared with that in other amorphous alloys [11–13]. This hydrogen-to-metal ratio is widely valid for non-covalent-type hydrides such as $TiFeH_2$ with a CsCl(B2)-type structure. Therefore, it is of importance to obtain accurate information on site occupations and thermal stabilities of hydrogen in MgNi. However, systematic investigations of neither X-ray and neutron diffraction measurements nor *P–C* (hydrogen pressure–composition) isotherm measurements have been carried out in the system so far.

Recently attention was paid to the Mg-site substitution in MgNi by elemental Al [14]. The reason is that Al forms a stable electron compound with a CsCl-type structure in the Al–Ni system around equiatomic composition [15]. Therefore, it is highly expected that a new crystalline phase with a CsCl-type structure is stabilized even in the Mg–Ni system by the Al-substitution of the Mg site, in agreement with the rule of the electron compound [16]. Al-substitution in MgNi corresponds to an increase of the number of valence electrons. Here it is worthy to note that as far as it is known the Al-substitution of the Mg in MgNi has never been realized by conventional melting methods, because the elemental Mg with a high vapor pressure cannot dissolve into the stable compound AlNi with a high melting temperature of nearly 2000 K.

The aim of this work is therefore to clarify the Al-substitution effects of MgNi on the structural and hydriding properties, also including the site occupations and thermal stabilities of hydrogen in MgNi itself.

2. EXPERIMENTAL PROCEDURES

2.1. Sample preparation

Mixtures of Mg_2Ni (nearly 300 μm powder size), Ni and Al (2–3 μm powder size) were mechanically alloyed under an argon atmosphere with a 5N5-purity, using a planetary ball mill apparatus (Fritsch P7) with 400 r.p.m. for 4800 min at room temperature. Here the compositional ratios were x = 0, 0.1, 0.2, 0.3, 0.4 and 0.5 for $(Mg_{1-x}Al_x)Ni$,

†To whom all correspondence should be addressed.
‡Present address: Max-Planck Institute für Metallforschung, Heisenbergstr. 1, 70569 Stuttgart, Germany.
§Present address: Matsushita Battery Industrial Co., Ltd, Moriguchi, Osaka 570-8511, Japan.
¶[Present address: Research Reactor Institute, Kyoto University Kumatori, Osaka 590-0494, Japan.

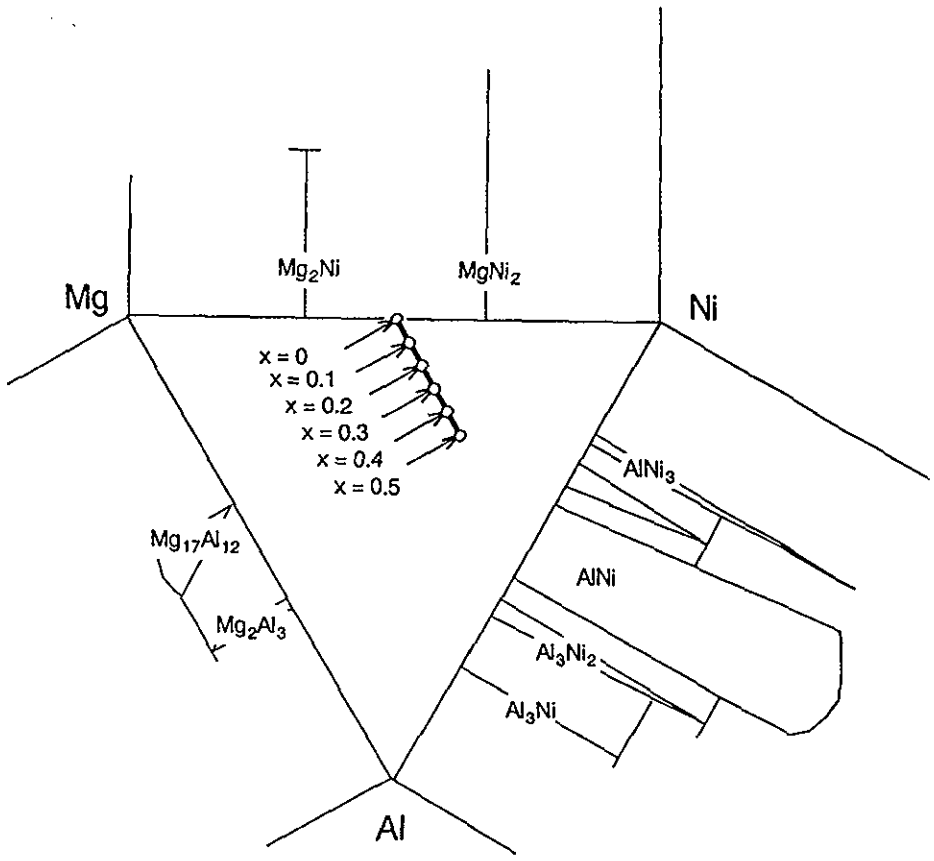

Fig. 1. Schematic phase diagram of the Mg–Al–Ni system.

as shown in Fig. 1. These ratios were checked by induction coupled plasma (ICP) spectrometry, and the compositional deviation of the samples between before and after mechanical alloying was less than 5% in any samples.

For the neutron diffraction measurements which will be described later, the sample with $x = 0$, MgNi, was fully deuterided under a deuterium atmosphere with a 4N-purity, using a Sieverts type apparatus under 1.0 MPa for 720 min at room temperature.

It should be emphasized that most attention was paid to avoid impurity effects on the structural and hydriding properties of the samples [17]; the material and shape of the vial for mechanical alloying were carefully selected, so as to lower the amount of the elemental Fe contaminated during mechanical alloying. In addition, the vial (equipped with a connection valve for evacuation or introduction of argon) with each sample was directly evacuated for 720 min below 0.01 Pa prior to mechanical alloying, and was always handled in a glove-box (filled with a purified argon of less than 0.5 p.p.m. oxygen, and of dew point lower than 185 K), so as to minimize oxidation and nitrogenation effects.

2.2. Sample characterization

The structural and hydriding properties of the sample thus prepared were characterized by X-ray (Cu-Kα radiation) and neutron diffraction measurements, differential thermal analysis, and electrochemical *P–C* isotherm measurement.

The differential thermal analysis was carried out under a purified argon atmosphere using a 30 mg sample and a heating rate of 5 K/min up to 773 K.

The neutron diffraction measurement of deuterided MgNi was carried out at room temperature by using a high intensity total scattering spectrometer (HITII) installed at a spallation pulsed neutron source generated from a 500 MeV proton booster synchrotron at the High Energy Accelerator Research Organization (KEK, Tsukuba, Japan) [18–20]. The sample of nearly 5 g was sealed under purified argon in a Ti–Zr cylindrical cell with a 0.35 mm thick wall, 8 mm inner diameter and 50 mm length. The diffracted neutron was detected by the time-of-flight method, and was normalized by the vanadium rod which is regarded as a perfect incoherent scatterer for neutrons. Duration of the measurement was 480 min for the sample, the empty cell, the vanadium rod and background, respectively.

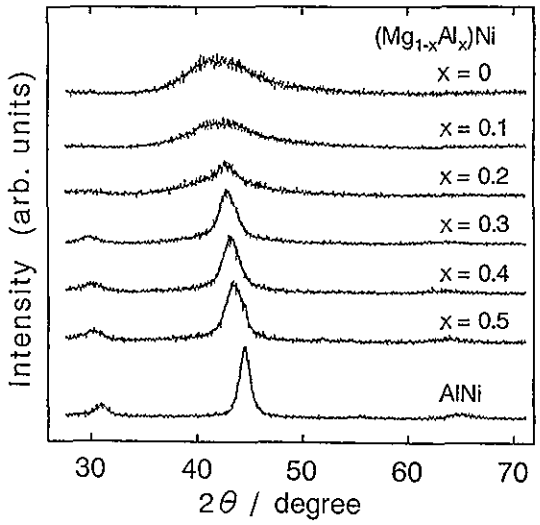

Fig. 2. X-ray diffraction profiles of $(Mg_{1-x}Al_x)Ni$ with x = 0, 0.1, 0.2, 0.3, 0.4 and 0.5. The profile of the intermetallic compound AlNi mechanically milled for 4800 min is also shown as a reference.

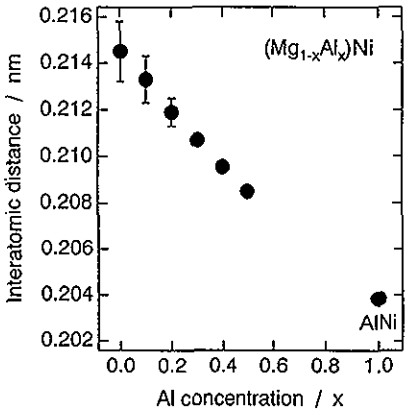

Fig. 3. Interatomic distances estimated from maximum positions of the halo profile (in x = 0, 0.1 and 0.2) and from (110) diffraction peaks (in x = 0.3, 0.4 and 0.5) shown in Fig. 2.

The electrochemical *P–C* isotherm measurement was carried out under the following conditions [21–23]; nearly 30 mg of the samples were mixed with Cu powder (< 63 μm) under air in the weights ratio of 1:3, and compressed under a pressure of 500 MPa to form a pellet 7 mm in diameter. The pellets were fixed with a cylindrical Teflon-clip on a Ni holder. The electrodes were electrochemically charged and discharged in a 6 M KOH electrolyte in an electrochemical cell open to the atmosphere. A nickel plate was used as counter electrode and potentials were referred to a Hg/HgO electrode. The discharge cut-off potential was −0.6 V with respect to the $Hg/HgO/OH^-$ reference electrode. After the full charge of the samples, the discharge processes were measured in equilibrium current with 20 mA/g, at room temperature.

3. RESULTS AND DISCUSSION

3.1. Structural properties of $(Mg_{1-x}Al_x)Ni$

Figure 2 shows the X-ray diffraction profiles of $(Mg_{1-x}Al_x)Ni$ with x = 0, 0.1, 0.2, 0.3, 0.4 and 0.5. The amorphous phase is formed in x = 0–0.2, while the crystalline phase of a CsCl-type structure is formed in x = 0.3–0.5. All the diffraction peaks are rather broad, which is not surprising for a crystalline phase composed of nanometer-scale crystallites with a high lattice defect concentration in the as-alloyed state.

Figure 3 shows the interatomic distances estimated from maximum positions of the halo profiles and from the (110) diffraction peaks in Fig. 2. This result indicates that interatomic distances in both the amorphous and crystalline phases continuously decrease with increasing Al concentration, reflecting that the atomic size of Al is 10% smaller than that of Mg.

The profiles of differential thermal analysis of $(Mg_{1-x}Al_x)Ni$ with x = 0, 0.1 and 0.3 are shown in Fig. 4. Upon heating MgNi, two exothermic reactions are observed; the first exothermic reaction at 596 K corresponds to the crystallization into Mg_2Ni, and the second one at 676 K into $MgNi_2$ [7, 11–13]. In x = 0.1, the two-step process still exists, although both exothermic reactions shift to nearly 30 K higher temperatures caused by the increment of activation energies for the crystallization [24, 25]. The peak area of each exothermic reaction in x = 0.1, especially that of the second one, decreases as compared with that in x = 0. This result qualitatively suggests that the amorphous phase in x = 0.1 is more stable than that in x = 0.

In contrast, little exothermic reaction corresponding to the crystallization is observed in x = 0.3 around the temperature ranges mentioned above. This result indicates that the crystalline phase with a CsCl-type structure is thermally stabilized at this composition.

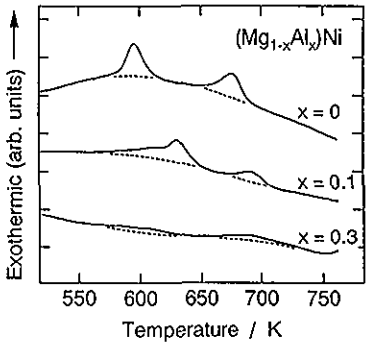

Fig. 4. Profiles of differential thermal analysis of $(Mg_{1-x}Al_x)Ni$ with x = 0, 0.1 and 0.3.

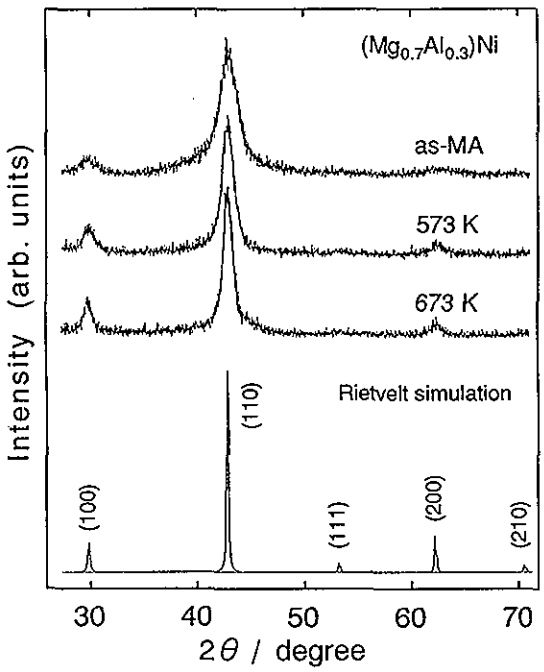

Fig. 5. X-ray diffraction profiles of heat-treated $(Mg_{0.7}Al_{0.3})Ni$. The Rietvelt simulation profile is also shown as a reference.

To confirm the thermal stability of the sample with $x = 0.3$, that is, $(Mg_{0.7}Al_{0.3})Ni$, it was heat-treated under a high-purity argon atmosphere, and the result of the X-ray diffraction is shown in Fig. 5. In this figure the diffraction peaks become sharp with increasing heat-treated temperatures, which comes from the grain growth and strain-release of crystallites. The positions and their intensity ratios of the (100), (110) and (200) diffraction peaks after the heat treatment at 673 K well correspond to those obtained from the Rietvelt simulation (RIETAN-94†) shown also in Fig. 5. In the simulation, it was assumed that the Mg-site of MgNi with the CsCl-type structure was randomly occupied by Al.

3.2. *Metal–deuterium correlation in MgNi–D*

X-ray and neutron diffraction profiles were analyzed to obtain accurate information on the metal–deuterium (Mg–D and Ni–D) correlations in *MgNi–D*. Prior to the analysis, the deuterium content in the deuterided sample was determined to be $MgNiD_{1.6}$ (3.8 wt%) by using the thermo gravimetric analysis, and the sample density was also determined to be 3.88 g/cm^3 by using high-sensitivity volumetric analysis.

The total structure factor for X-ray diffraction $S(Q)^X$ and that for neutron diffraction $S(Q)^N$ are shown in Fig. 6. Here, the scattering vector Q is expressed as $4\pi \sin\theta/\lambda$, using the scattering angle 2θ and the wavelength λ. The total structure factor $S(Q)$ is defined [26] as

$$S(Q) = W_{MgMg}S_{MgMg}(Q) + W_{NiNi}S_{NiNi}(Q) + W_{DD}S_{DD}(Q) + W_{MgNi}S_{MgNi}(Q) + W_{MgD}S_{MgD}(Q) + W_{NiD}S_{NiD}(Q). \quad (1)$$

Here, for example, $S_{MgMg}(Q)$ is the partial structure factor for the Mg–Mg pair, and W_{MgMg} is the weighting factor for the atom pair defined as

$$W_{MgMg} = (c_{Mg}^2 f_{Mg}^2)/(c_{Mg}f_{Mg} + c_{Ni}f_{Ni} + c_D f_D)^2 \quad (2)$$

using the atomic concentration c and the atomic scattering factor f for X-rays (or the mean coherent scattering length b for neutrons, instead of f). Therefore, after a simple calculation

$$S(Q)^X = 0.0833S_{MgMg}(Q) + 0.4533S_{NiNi}(Q) + 0.0015S_{DD}(Q) + 0.3885S_{MgNi}(Q) + 0.0220S_{MgD}(Q) + 0.0514S_{NiD}(Q) \quad (3)$$

for X-ray diffraction, and

$$S(Q)^N = 0.0419S_{MgMg}(Q) + 0.1538S_{NiNi}(Q) + 0.1626S_{DD}(Q) + 0.1605S_{MgNi}(Q) + 0.1650S_{MgD}(Q) + 0.3162S_{NiD}(Q) \quad (4)$$

for neutron diffraction.

The Fourier transformation of $S(Q)$ gives the total radial distribution function defined [19] as

$$RDF(r) = 4\pi r^2 \rho_0 g(r) \quad (5)$$

where

$$g(r) = 1 + 1/(2\pi r^2 \rho_0)\int_0^Q Q[S(Q) - 1]\sin Qr\, dQ \quad (6)$$

and ρ_0 is the mean number density derived from the sample density mentioned above. The total

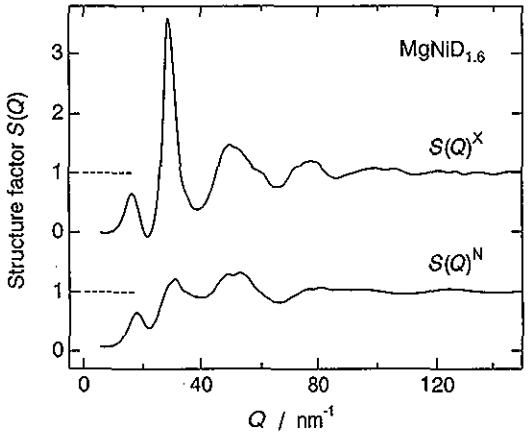

Fig. 6. Total structure factor for X-ray diffraction $S(Q)^X$ and that for neutron diffraction $S(Q)^N$ of $MgNiD_{1.6}$.

†RIETAN-94 prepared by F. Izumi, and installed as the application software of the X-ray diffraction apparatus, Mac Science MPX3.

radial distribution function for X-ray diffraction $RDF(r)^X$ and that for neutron diffraction $RDF(r)^N$ are also presented by the weighted sum of the partial radial distribution functions as follows:

$$RDF(r)^X = 0.0833RDF_{MgMg}(r) + 0.4533RDF_{NiNi}(r) + 0.0015RDF_{DD}(r) + 0.3885RDF_{MgNi}(r) + 0.0220RDF_{MgD}(r) + 0.0514RDF_{NiD}(r) \quad (3')$$

and

$$RDF(r)^N = 0.0419RDF_{MgMg}(r) + 0.1538RDF_{NiNi}(r) + 0.1626RDF_{DD}(r) + 0.1605RDF_{MgNi}(r) + 0.1650RDF_{MgD}(r) + 0.3162RDF_{NiD}(r). \quad (4')$$

The results of Fourier transformation truncated at $Q = 150$ nm are shown in the upper part of Fig. 7. The large single peak around $r = 0.270$ nm in the $RDF(r)^X$ corresponds to the metal–metal (Mg–Mg, Mg–Ni and Ni–Ni) correlations; it is impossible to accurately estimate the contribution of the metal–deuterium (Mg–D and Ni–D) correlations coming from their small weighting factors shown in equation (3'). In the $RDF(r)^N$, however, the metal–deuterium (Mg–D and Ni–D) correlation, especially the Ni–D correlation around $r = 0.174$ nm, is clearly visible due to their large weighting factors shown in equation (4'), although the positions of the Mg–D correlation is close to the Ni–Ni correlation. In order to clarify also the Mg–D correlations, therefore, the contribution of the Ni–Ni correlation was eliminated using equations (3') and (4') as follows:

$$RDF(r)^{N-X} = \{(RDF(r)^N)/0.1538 - (RDF(r)^X)/0.4533\}/(1/0.1538 - 1/0.4533) = 0.0206RDF_{MgMg}(r) + 0.2453RDF_{DD}(r) + 0.0434RDF_{MgNi}(r) + 0.2384RDF_{MgD}(r) + 0.4522RDF_{NiD}(r). \quad (7)$$

In this equation, the contributions from the Mg–Mg and Mg–Ni correlations amount to only 2.1 and 4.3%, respectively. The lower part of Fig. 7 shows the $RDF(r)^{N-X}$, that is, the profile of equation (7).

Table 1. The coordination numbers n and interatomic distances r of the Mg–D and Ni–D correlation in $MgNiD_{1.6}$

	n	r
Mg–D	2.3 ± 0.3	0.218 ± 0.003 nm
Ni–D	1.7 ± 0.3	0.164 ± 0.003 nm

The coordination numbers n and interatomic distances r of the Mg–D and Ni–D correlations in MgNi–D were determined by least-squares fitting using Gaussian peak profiles shown in Fig. 7, which are summarized in Table 1. This table directly shows that deuterium in MgNi–D occupies the tetrahedral site composed of nearly 2Mg2Ni, and implies that the local atomic structure is also similar to the CsCl-type structure at least in deuterided (hydrogenated) state at room temperature. In Mg_2NiD_4, deuterium occupies the 4Mg1Ni site [27] due to the formation of the stable covalent-type bonding composed of Mg^{2+} and $[NiD_4]^{4-}$ complex [2–5]. In addition, it is also of importance that the Ni–D distances in MgNi–D are obviously enlarged compared with that in Mg_2NiD_4 with the $[NiD_4]^{4-}$ complex, 0.149 nm [27]. Therefore, the interstitial 2Mg2Ni-site occupation indicates that the chemical bonding of deuterium (hydrogen) is weakened in MgNi–D compared with that in Mg_2NiD_4. X-ray photoelectron spectroscopic studies are underway to evaluate the nature of the chemical bonding.

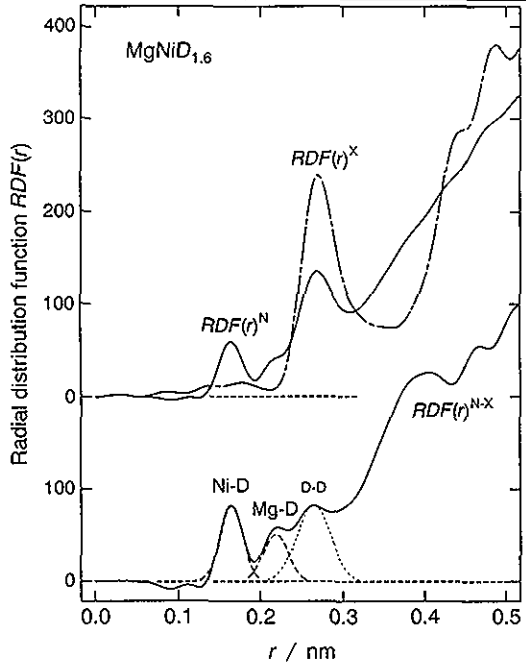

Fig. 7. Upper part: total radial distribution function for X-ray diffraction $RDF(r)^X$ and that for neutron diffraction $RDF(r)^N$ of $MgNiD_{1.6}$. Lower part: subtracted total radial distribution function $RDF(r)^{N-X}$ of $MgNiD_{1.6}$.

3.3. Hydriding properties of $(Mg_{1-x}Al_x)Ni$

The electrochemical *P–C* isotherm of $(Mg_{1-x}Al_x)Ni$ with $x = 0$, 0.1 and 0.3 are shown in Fig. 8. The maximum hydrogen contents shown in Fig. 8 agree well with those of the same samples hydrogenated by the gas-charge process. For example, the hydrogen content in $x = 0$ corresponds to $MgNiH_{1.7}$ (2.0 wt%) under a hydrogen pressure of 5×10^{-3} MPa in Fig. 8, while the value was $MgNiH_{1.9}$ (2.2 wt%) under 1 MPa as previously reported [11–14].

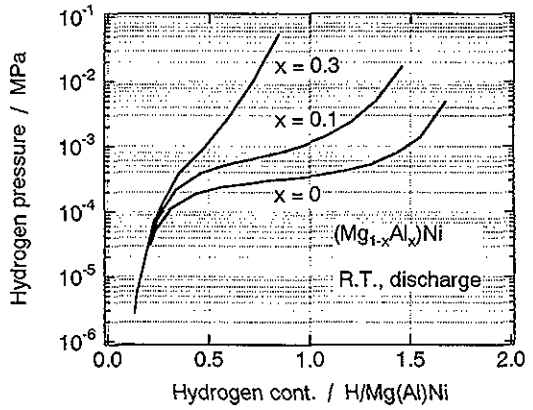

Fig. 8. Electrochemical *P–C* (hydrogen pressure–composition) isotherm of $(Mg_{1-x}Al_x)Ni$ with $x = 0$, 0.1 and 0.3 (in the discharge process at room temperature).

One of the interesting hydriding properties is that there is obviously the miscibility-gap (plateau) pressure even in $x = 0$, that is, even in the amorphous phase. Here, the pressure change of the plateau region is no more than a factor of four. So far, conventional amorphous phases, such as ZrNi, have no plateau pressure due to their wide hydrogen-site stabilities [28–31]. The width dominantly comes from the variation of neighboring metal atoms around hydrogen atoms. In the amorphous phase of ZrNi, for example, there are several types of nearest metal coordinations with different hydrogen-site stabilities, from 4Zr to 1Zr3Ni or 4Ni. In contrast, the restricted type of nearest metal coordinations, like 2Mg2Ni described in Section 3.2, realizes in MgNi to have the narrow range of hydrogen-site stabilities, corresponding to the *P–C* isotherm shown in Fig. 8.

It should be also noted that the miscibility-gap pressure of MgNi locates around 3×10^{-4} MPa at room temperature. In Mg_2NiH_4 with stable covalent-type bonding composed of Mg^{2+} and $[NiH_4]^{4-}$ complex, the plateau pressure extrapolated to room temperature is of the order of 10^{-6} MPa [32]. These hydriding properties attribute to the different metal–D(H) correlations between that in MgNi–D(H) and in Mg_2NiH_4 described in Section 3.2. Furthermore, the results of the high-resolution proton NMR measurements [33] agree well with the above hydriding properties; that is, the local environments of hydrogen in MgNi–H exhibit an intermediate character between those in Mg_2NiH_4 with stable covalent-type bonding and in $(\alpha\text{-})Mg_2NiH_{0.3}$ with weak metallic bonding of the hydrogen solution.

Moreover, Fig. 8 also shows that the miscibility-gap pressure increases from $x = 0$ to 0.1, and reaches almost 1×10^{-3} MPa. The pressure increase is related to the decrease of interatomic distances shown in Fig. 3, and from the lower affinity of elemental Al with hydrogen [34]. In $x = 0.3$, the slope of the isotherm becomes steep. Heat treatments for both the grain growth and strain-release of crystallites are necessary for further improvements of the hydriding properties.

4. CONCLUSIONS

The amorphous phase is formed in $(Mg_{1-x}Al_x)Ni$ with $x = 0$–0.2, while the crystalline phase of a CsCl(B2)-type cubic structure is formed with $x = 0.3$–0.5. The coordination numbers and interatomic distances of the Mg–D and Ni–D correlations in MgNi–D show that deuterium occupies the interstitial tetrahedral site composed of nearly 2Mg2Ni. The electrochemical *P–C* (hydrogen pressure–composition) isotherm measurements of $(Mg_{1-x}Al_x)Ni$ revealed the following results: there is obviously a miscibility-gap pressure higher than 10^{-4} MPa at room temperature even in MgNi, and the pressure increases by Al-substitution.

Acknowledgements—A part of this work was financially supported from the New Energy and Industrial Technology Development Organization (NEDO) as an International Collaboration Work Project for New Materials.

REFERENCES

1. Percheron-Guégan, A. and Welter, J.-M., in *Topics in Applied Physics, Vol. 63, Hydrogen in Intermetallic Compounds I*, ed. L. Schlapbach. Springer-Verlag, Berlin, 1988, p. 11.
2. Yvon, K., *J. less-common Metals*, 1984, **103**, 53.
3. Gupta, M. and Schlapbach, L., in *Topics in Applied Physics, Vol. 63, Hydrogen in Intermetallic Compounds I*, ed. L. Schlapbach. Springer-Verlag, Berlin, 1988, p. 139.
4. Noréus, D., Jansson, K. and Nygre, M., *Z. phys. Chem.*, 1985, **146**, 191.
5. Takahashi, Y., Yukawa, H. and Morinaga, M., *J. Alloys Comp.*, 1996, **242**, 98.
6. Reilly, J. J. and Wiswall Jr, R. H., *Inorg. Chem.*, 1968, 7, 2254. Recently, it has been experimentally confirmed that the mechanical grinding method promotes a hydriding reaction of the $MgNi_2$.
7. Yang, Q. M., Lei, Y. Q., Chen, C. P., Wu, J., Wang, Q. D., Lu, G. L. and Chen, L. S., *Z. phys. Chem.*, 1994, **183**, 141.
8. Sun, D. L., Lei, Y. Q., Liu, W. H., Jiang, J. J., Wu, J. and Wang, Q. D., *J. Alloys Comp.*, 1995, **231**, 621.
9. Iwakura, C., Nohara, S., Inoue, H. and Fukumoto, Y., *Chem. Commun.*, 1996, **15**, 1831.
10. Liu, W. H., Wu, H. Q., Lei, Y. Q. and Wang, Q. D., *J. Alloys Comp.*, 1997, **252**, 234.
11. Orimo, S., Ikeda, K., Fujii, H., Fujikawa, Y., Kitano, Y. and Yamamoto, K., *Acta mater.*, 1997, **45**, 2271.
12. Orimo, S., Fujii, H., Ikeda, K., Fujikawa, Y. and Kitano, Y., *J. Alloys Comp.*, 1997, **253-254**, 94.
13. Orimo, S. and Fujii, H., *Intermetallics*, 1998, **6**, 185.
14. Orimo, S., Ikeda, K. and Fujii, H., *J. Alloys Comp.*, 1998, **266**, L1.
15. See, e.g. de Boer, F. R., Boom, R., Mattens, W. C. M., Miedema, A. R. and Niessen, A. K., *Cohesion in Metals—Transition Metal Alloys*. North-Holland, Amsterdam, 1988, p. 309.

16. Hume-Rothery, W., *Electrons, Atoms, Metals and Alloys*, 3rd revised edn. Dover, New York, 1963, p. 314.
17. Orimo, S., Fujii, H. and Ikeda, K., *Acta mater.*, 1997, **45**, 331.
18. Suzuki, K., Misawa, M., Kai, K. and Watanabe, N., *Nucl. Instrum. Meth.*, 1977, **147**, 519.
19. Fukunaga, T., Ph.D. thesis, Tohoku University, 1978.
20. Fukunaga, T., *Physica B*, 1995, **213**, 518.
21. Züttel, A., Meli, F. and Schlapbach, L., *J. Alloys Comp.*, 1994, **203**, 235.
22. Züttel, A., Meli, F. and Schlapbach, L., *J. Alloys Comp.*, 1995, **231**, 645.
23. Züttel, A., Chartouni, D., Gross, K., Bächler, M. and Schlapbach, L., *J. Alloys Comp.*, 1997, **253-254**, 587.
24. Buschow, K. H. J. and Beekmans, N. M., *Solid St. Commun.*, 1980, **35**, 233.
25. Orimo, S., Ikeda, K., Fujii, H. and Yamamoto, K., *J. Alloys Comp.*, 1997, **260**, 143.
26. Faber, T. E. and Ziman, J. M., *Phil. Mag.*, 1965, **11**, 153.
27. Yvon, K. and Fischer, P., in *Topics in Applied Physics, Vol. 63, Hydrogen in Intermetallic Compounds I*, ed. L. Schlapbach. Springer-Verlag, Berlin, 1988, p. 87.
28. Spit, F. H. M., Drijver, J. W. and Radelaar, S., *Scripta metall.*, 1980, **14**, 1071.
29. Kirchheim, R., Sommer, F. and Schluckebier, G., *Acta metall. mater.*, 1982, **30**, 1059.
30. Aoki, K., Kamachi, M. and Masumoto, T., *J. Non-Cryst. Solids*, 1984, **61/62**, 679.
31. Harris, J. H., Curtin, W. A. and Tenhover, M. A., *Phys. Rev. B*, 1987, **16**, 5784.
32. Nomura, K., Akiba, E. and Ono, S., *Int. J. Hydrogen Energy*, 1981, **6**, 295.
33. Hayashi, S., Orimo, S. and Fujii, H., *J. Alloys Comp.*, 1997, **261**, 145.
34. Griessen, R. and Riesterer, T., in *Topics in Applied Physics, Vol. 63, Hydrogen in Intermetallic Compounds I*, ed. L. Schlapbach. Springer-Verlag, Berlin, 1992, p. 266.